Journal of Power Sources 196 (2011) 6160–6167

Contents lists available at ScienceDirect

Journal of Power Sources

journal homepage: www.elsevier.com/locate/jpowsour

Platinum decorated aligned carbon nanotubes: Electrocatalyst for improved performance of proton exchange membrane fuel cells

Yuan Yuan[a], Joshua A. Smith[b], Gabriel Goenaga[c], Di-Jia Liu[d,**], Zhiping Luo[e], Jingbo Liu[b,f,g,*,1]

[a] Department of Environmental Engineering, Texas A&M University-Kingsville, MSC 213, Kingsville, TX 78363-8012, United States
[b] Department of Chemistry, Texas A&M University-Kingsville, MSC 161, Kingsville, TX 78363-8012, United States
[c] Chemical and Biomolecular Engineering, University of Tennessee, Knoxville, TN 37996, United States
[d] Chemical Sciences and Engineering Division, Argonne National Laboratory, Argonne, IL 60439-4837, United States
[e] Microscopy and Imaging Center and Materials Science and Engineering Program, Texas A&M University, 2257 TAMU, College Station, TX 77843, United States
[f] Department of Chemistry, Texas A&M University, P.O. Box 30012, College Station, TX 77842-3012, United States
[g] Department of Materials Science and Engineering, The University of Tokyo, 7-3-1 Hongo, Bunkyo-ku, Tokyo 113-8656, Japan

ARTICLE INFO

Article history:
Received 19 January 2011
Received in revised form 11 March 2011
Accepted 12 March 2011
Available online 22 March 2011

Keywords:
Aligned carbon nanotubes
Platinum nanoparticles
Proton exchange membrane fuel cells
Amphiphilic modification
Nanostructural characterization
Electrochemical performance

ABSTRACT

This study aims to improve the performance of proton exchange membrane fuel cells (PEMFCs) using carbon nanotubes as scaffolds to support nanocatalyst for power generation over prolonged time periods, compared to the current designs. The carbon nanotubes are prepared using chemical vapor deposition and decorated by platinum nanoparticles (Pt-NPs) using an amphiphilic approach. The PEMFC devices are then constructed using these aligned carbon nanotubes (ACNTs) decorated with Pt-NPs as the cathode. The electrochemical analyses of the PEMFC devices indicate the maximum power density reaches to 860 mW cm^{-2} and current density reaches 3200 mA cm^{-2} at 0.2 V, respectively, when O_2 is introduced into cathode. Importantly, the Pt usage was decreased to less than 0.2 mg cm^{-2}, determined by X-ray energy dispersive spectroscopy and X-ray photoelectron spectroscopy as complimentary tools. Electron microscopic analyses are employed to understand the morphology of Pt-ACNT catalyst (with diameter of 4–15 nm and length from 8 to 20 μm), which affects PEMFC performance and durability. The Pt-ACNT arrays exhibit unique alignment, which allows for rapid gas diffusion and chemisorption on the catalyst surfaces.

1. Introduction

Proton exchange membrane fuel cells (PEMFCs) are one of the most important green energy conversion devices due to their high power density, energy conversion efficiency, flexible design and zero or near-zero emission to the environment [1–4]. The PEMFCs are composed of membrane electrode assembly (MEA), including a polymeric membrane electrolyte (commercially available Nafion 212 has been used in this study) in the center, and an anode and a cathode at each side [5–8]. On the anode compartment, fuel supplies, such as hydrogen (H_2) are oxidized to proton (H^+), whereas, oxidants, such as oxygen (O_2) are reduced on the cathode side [9–11]. The electrons travel from anode to cathode externally to provide direct current for stationary and portable application [12,13]. The H^+ ions transfer from the anode through the Nafion electrolyte and react with the O_2 to form water at the cathode surface through oxygen reduction reaction or ORR ($4H^+ + O_2 + 4e^- \rightarrow 2H_2O$) [14,15].

Current design of the PEMFC encounters some problems, such as: materials compatibility, high material/manufacturing cost, and performance degradation over prolonged use, which collectively hinders widespread adaptation and commercialization [16,6,17]. To improve PEMFC performance and durability, and to lower catalyst cost, a great number of studies have focused on building new and robust anode and cathode catalysts [18–20]. The commonly used catalyst, Pt/C has been used for decades due to its high catalytical reactivity; however its expense is a major concern [21–23]. Recently, alternative supports have been applied to improve corrosion resistance, mass transfer and to reduce Pt loading. One of the most attractive catalyst-support materials is carbon nanotubes (CNTs) due to their large surface areas, high chemical stability, high electric conductivity and extraordinary mechanical strength [24–27]. In general, CNTs are coaxial cylinders of graphite sheets, which allow for the structural diversity.

* Corresponding author at: Department of Chemistry, Texas A&M University, P.O. Box 30012, College Station, TX 77842-3012, United States. Tel.: +1 361 5932919; fax: +1 361 5933597.
** Corresponding author.
E-mail addresses: yuan.yuan@students.tamuk.edu (Y. Yuan), joshua.smith@students.tamuk.edu (J.A. Smith), ggoenaga@utk.edu (G. Goenaga), djliu@anl.gov (D.-J. Liu), luo@mic.tamu.edu (Z. Luo), kfjll00@tamuk.edu, jingbo.liu@chem.tamu.edu (J. Liu).
[1] JSPS Invitation Fellow (short-term).

0378-7753/$ – see front matter © 2011 Elsevier B.V. All rights reserved.
doi:10.1016/j.jpowsour.2011.03.026

The most important structures of CNTs are single-walled nanotubes (SWNTs), multiwalled nanotubes (MWNTs), and aligned carbon nanotubes (ACNTs) [28–33]. The CNTs can be fabricated by carbon-arc discharge, laser ablation, and chemical vapor deposition [34–37]. Moreover, to increase the Pt specific surface area and lower its cost, highly dispersed Pt-NPs have been employed as catalysts supported by CNTs to facilitate the ORR process. ORR is the rate limiting step, which dominates the PEFMC efficiency due to its 4-electron involvement and large activation energy for reaction [38–41].

In the present study, Pt-ACNTs cathodic catalyst and MEA performance were investigated to optimize PEMFC catalyst fabrication methodology. This differs from other approaches, which have had issues with stability of the Pt-support [42] or large Pt size [43], which in turn can affect overall reactivity of cathode catalyst [44]. Therefore, ACNT supports have been fabricated to replace traditional carbon black-based catalysts [45]. The rationale to use CNTs lies on the facts that the sp^2 hybridization of carbon atoms provides high mechanical strength and also allows for the p electron in carbon atoms to be transferred to the unoccupied d-orbital of Pt. This phenomenon can further enhance the interactions between ACNT and Pt atoms, which reinforce the stability of the cathode materials under oxidative environment [26,46–48]. In addition to the stability of Pt-decorated ACNTs, the hydrophobicity of the ACNTs can prevent cathode flooding and favour water management, which consequently improves gas transport in the PEMFC electrode [49–51]. The Pt-ACNTs have orderly structure which can be tuned into the electrode support with high triple phase boundary (TPB) between cathode, electrolyte membrane and gas reactants. With the increase of TPB, the increased electrochemical behaviour of the PEMFC devices is anticipated [52,53]. The contributions of this research are: (1) synthesis of ACNTs by the chemical vapor deposition (CVD) method to support Pt catalyst for ORR and to prevent cathode flooding; (2) decoration of ACNTs by Pt NPs through a novel and feasible amphiphilic chemical impregnation, followed by heat treatment; (3) integration of advanced analytical instrumentation techniques into PEMFCs electrochemical performance measurement.

2. Materials and methods

All reagents, chemicals and solvents were obtained from VWR International (West Chester, PA) and Sigma–Aldrich (St Louis, MO) to prepare the nanotubes and construct membrane electrode assemblies (MEAs), unless otherwise specified. The reagents were reagent grade and were used without further purification. Doubly distilled and 0.2 μm filtered (Milli-Q) water was used in the dissolution of reactants. State-of-the-art facilities were used to characterize the nanostructure and electrochemical performance. The commercial MEA was procured from BASF Corporation (Port Arthur, TX) for comparative study, with loading of 0.5 mg Pt cm^{-2} on both electrodes.

2.1. Nanocatalyst fabrication

The ACNTs were produced via the chemical vapor deposition (CVD) method. The main reactants were ferrocene ($Fe(C_5H_5)_2$) and xylene (C_8H_{10}). The quartz glass slides (with 5 cm^2 surface areas) were used as substrates for ACNT growth positioned inside of a quartz tube surrounded by a tube furnace with two independently controlled temperature zones. In the first zone, reactants (ferrocene and xylene solution) were injected at a rate of 0.225 or 0.250 mL min^{-1} and vaporized at 225 °C. In the second zone, the reactant molecules from the vaporized solution were decomposed over the seed of iron (Fe) particles to form nanotubes. Under the precise control of temperature, injection flow rate of reactants, and flow rate of inert gas (Ar) and hydrogen mixture, ACNTs with well-arranged arrays grew on the substrates. The Fe from ferrocene was continually fed as "seed", on which the carbon could accumulate into multiwalled tubes. ACNTs were then functionalized by Pt using wet impregnation. Several Pt-containing precursors, such as chloroplatinic acid hexahydrate ($H_2PtCl_6{\cdot}6H_2O$), platinum(II) acetylacetonate ($Pt(acac)_2$), platinum(IV) sulfite ($Pt(SO_3)_2$), and tetraammineplatinum(II) nitrate ($Pt(NH_3)_4(NO_3)_2$) were used to obtain mono-dispersed Pt nanoparticles. The Pt-modified ACNTs were activated by the heat treatment at 300 °C for 1 h under reducing atmosphere (H_2). This process termed reduction, which also contributed to removal of the impurities in ACNTs. Next, ACNT catalyst was sprayed with Nafion solution with mass ratio of 1:1 (Nafion to ACNTs).

The ACNT-based membrane electrode assembly (MEA) fabrication has been previously reported [37,52] and its geographical surface area was kept at 5.0 cm^2. The decal for anode consisted of a polymer substrate with a thin layer of teflon coating, painted with an ink composed of carbon-loaded Pt. The ink consisted of tetrabutylammonium hydroxide, Pt 20% (w/w), Nafion (w/w) 5%, and glycerol. The anode decal was placed into an oven heated to 140 °C for approximately an hour between each painting step. The painting–heating cycle was typically repeated up to five times or until the total weight of wet ink reached 8.00 mg. The sample was then left in the oven overnight and usually yielded a desired weight of 7.00 mg of anode catalyst, which corresponds to 0.2 mg Pt cm^{-2} loading. The anodic and cathodic substrates were then placed on two sides of the Na-form Nafion 212 membrane with the thickness averaged at 50 μm. Hot pressing technique was then used to fabricate the MEA under temperature of 210 °C and pressure of 600 pounds-per-square-inch-gauge (psig) for 5–10 min. The teflon (support for anode) and glass substrate (support for cathode) were then carefully removed from the MEA, which was subsequently treated in boiling H_2SO_4 (0.5 M) aqueous solution for 1–2 h. The H_2SO_4 acid treatment aims to exchange Na^+ by H^+ to increase the proton conductivity. The MEA was then washed in boiled distilled water for 1 h to remove the Na^+, Fe^{2+} and other impurities.

2.2. Nanocatalyst characterization

The nanostructure and elemental composition of the Pt-ACNT catalysts and MEA were characterized using several characterization techniques. The surface morphology, cross-sectional images and the thickness of the aligned carbon nanotubes were determined using a field emission scanning electron microscope (JSM-6701F) equipped with X-ray energy dispersive spectroscope (EDS, Department of Chemistry, Texas A&M University-Kingsville). An accelerating voltage of 20 kV and high vacuum of about 1.0×10^{-5} mbar were generally employed. The substrate of cathode and MEA were mechanically fractured using a razor blade, enabling an easier estimation of the PEMFC thickness. The high resolution TEM (Tecnia F20-G^2) equipped with post-column Gatan Image Filter was applied, and magnifications were calibrated using standards of commercial cross-line grating replica and silicon carbide (SiC) lattice images to obtain images and electron diffraction patterns with high accuracy and resolution [54]. Raman spectroscopic analysis was conducted to evaluate the vibration mode and electron structure of Pt and ACNTs. Raman/Fourier transform infrared spectroscopy with confocal microscope (Hariba Jobin–Yvon LabRam IR system, Texas A&M University-College Station) was employed to obtain highly specific fingerprints to enable precise chemical and molecular characterization and identification. Raman module used was fiber optic coupled with the laser excitation lines of 632 nm with the scan range of

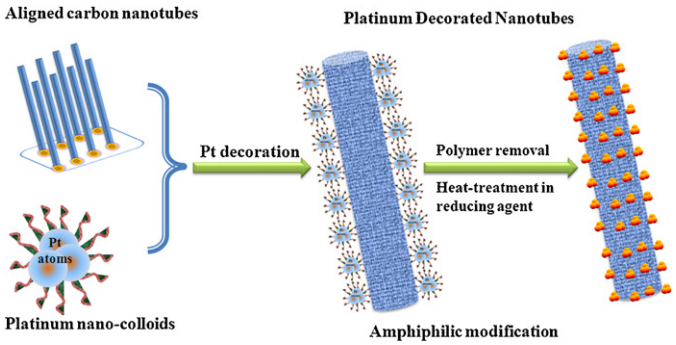

Fig. 1. The amphiphilic wet-chemistry approach to decorate ACNT using Pt nanoparticles, followed by reduction under H_2 atmosphere at 300 °C.

100–3000 cm^{-1}. The resolution was kept at 0.3 cm^{-1} per pixel for various lines.

2.3. Electrochemical performance measurement

The evaluation of PEMFC single cell performance with ACNT-based MEA was carried out using a commercially available test stand (Fuel Cell Technologies, Albuquerque, NM) and lab-assembled test stand. The pressurized and humidified H_2 and O_2 (air) were fed into the anode and cathode chambers as the fuel and oxidant under various flow rates. The cell operating conditions were controlled at various temperatures ranging from 70 °C to 90 °C. Typically, the H_2 flow rate was set at 100 mL min^{-1} and flow rate of O_2 at 300 mL min^{-1} with the back pressure at 14.0 psig for both cathode and anode compartments. The potential sweeps were controlled at fast rate with 5 s duration or slow rate with 30 s duration per datum point. The data were collected using LabVIEW 7 software™. The cell voltage drop originating from the electrolyte resistance was not compensated in this study. The relationship between cell current density and power density as function of applied potential was established for estimation of PEMFC performance. The cell was generally purged by safe gas at anode and air at cathode at ambient temperature prior to the electrochemistry study. The conditioning of the PEMFC was conducted for 16 h before direct current (DC) polarization was performed.

3. Results and discussions

The Pt-decoration of ACNTs using amphiphilic wet chemical approach and their characterization using microscopic and spectroscopic techniques are described. The electrochemical performance of the PEMFC devices constructed using Pt-ACNTs as cathode, Nafion as electrolyte membrane and Pt-loaded carbon graphite as anode is tested using fuel cell test station and the importance of the findings is summarized.

3.1. Pt-decoration of ACNT

In general, periodically aligned carbon nanotubes (ACNTs) can be synthesized with tunable pore diameters and rigid structural order using iron (Fe) as catalyst. The self assembly of multiwalled ACNTs with uniform ordered nanopores can be achieved. Importantly, the spacing between individual CNTs provides efficient channel for gas molecule transport. To improve the electrocatalytical activity, ACNTs must be modified using Pt-NPs. However, high dispersion and ultrafine Pt-NPs with high stability are extremely difficult to obtain due to poor wettability over hydrophobic ACNT by aqueous based precursor solution. Therefore, we focused on new catalyzing process to optimize the deposition of Pt-NPs on the surface of ACNTs. Conducting a series of experiments, we developed an amphiphilic wet-chemistry procedure (Fig. 1) to decorate and functionalize ACNTs. The two key points in this process are: (1) to maintain the distinctive alignment of well-channelled ACNT and (2) to dissolve the H_2PtCl_6 in aqueous solution for monodispersion and homogeneity. Therefore, hydrophilic and hydrophobic agents are needed to achieve the above goals. The critical step for this advancement is the modification of ACNT cathode catalyst using homogenous Pt-NPs, while the ACNTs alignment is well-maintained. This can be accomplished using a novel method, defined as "amphibious functionalization", in which the aromatic conjugate ring of the nanotube surfaces can then be functionalized by hydroxyl group, which forms ion-dipole intermolecular forces with Pt^{4+} cations.

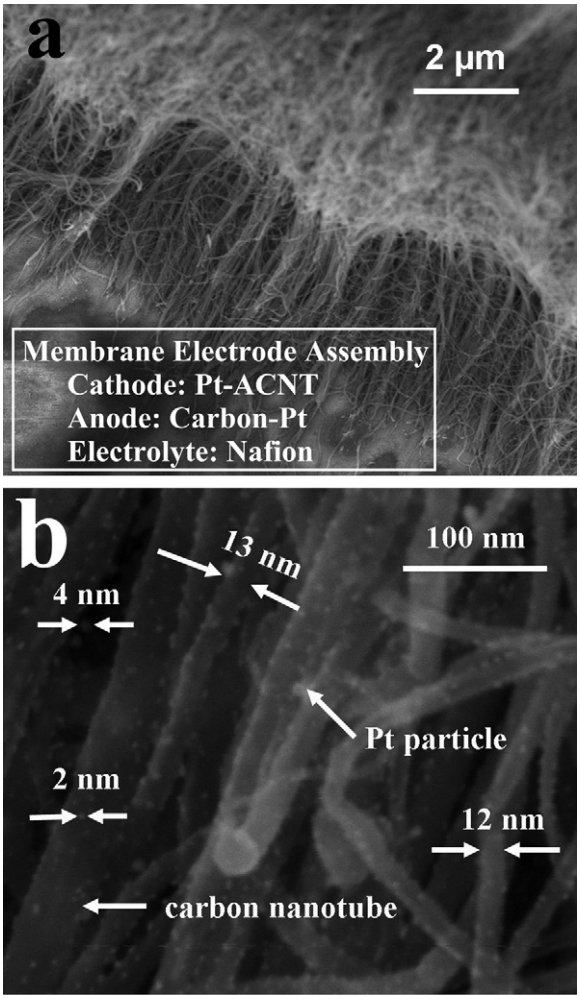

Fig. 2. Scanning electron microscopic analyses of the MEA composed of Pt-functionalized ACNT. (a) The Pt-ACNT aligned structure maintained well and (b) Pt nanoparticles averaged at size of 2–4 nm before the electrochemical study is conducted.

Two reagents, namely isopropanol (C_3H_7OH) and distilled water, which are miscible, were used to control the homogeneity from the molecular level. The focus centers on optimization of the Pt starting materials, dispersing agents, amount of the Pt mass, and Pt particle size. Firstly, the ACNT surfaces need to be functionalized using amphiphilic solvent (isopropanol containing 1 mol% of Nafion) to maintain its geometry and provide hydroxyl (OH) group. The water-soluble Pt^{4+} compound (such as H_2PtCl_6) is then sprayed onto the surface of ACNT. Due to intermolecular forces (such as ion-dipole coupling), the Pt^{4+} can then interact with ACNT and retain its alignment. Secondly, step-wise deposition of metallic cations onto charged ACNT surface assists self-assembly of amphiphilic

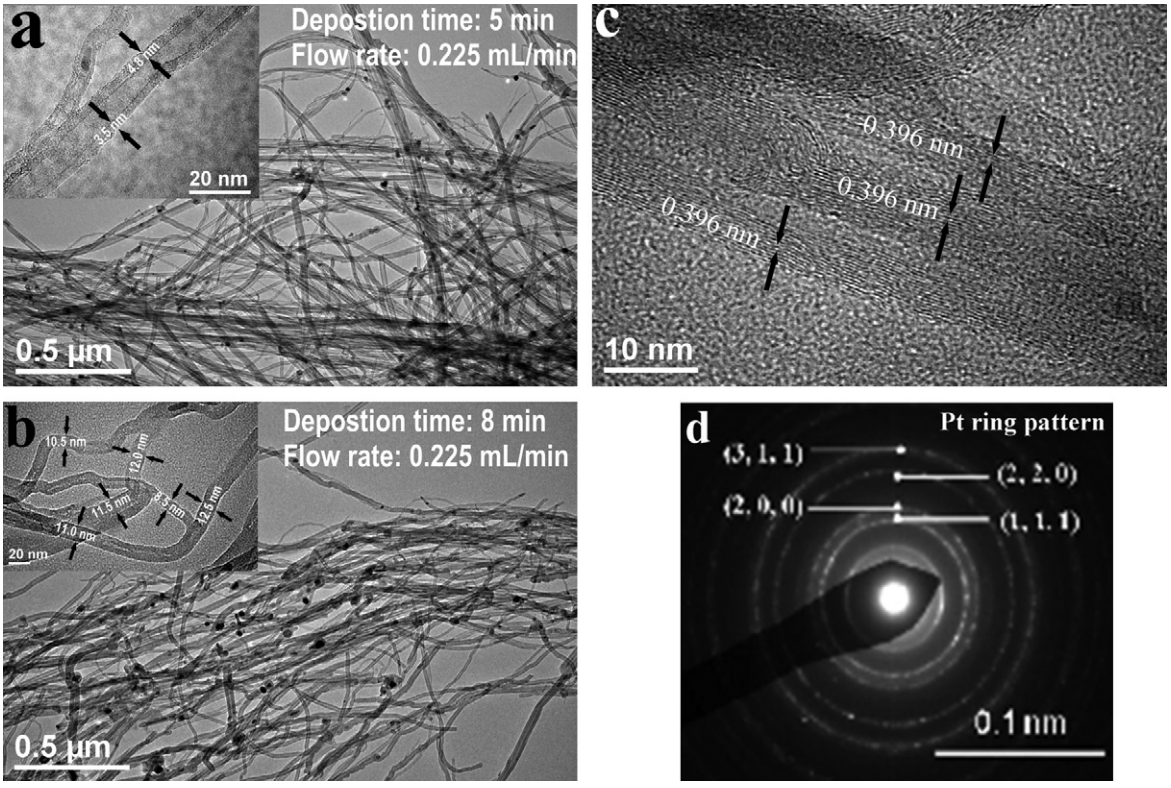

Fig. 3. Transmission electron microscopic analyses of the MEA composed of Pt-functionalized ACNT. (a) ACNT display narrower diameter when deposition was controlled at 5 min; (b) ACNT display wider diameter when deposition was controlled at 8 min; (c) the distance between multiwall nanotubes; (d) Pt ring pattern showing crystalline Pt formed.

block copolymers followed by formation of covalent bond with the ACNT "backbones". Lastly, graft copolymerization onto reactive seeded particles will allow cations to link with the ACNT backbones. Through polymer crafting and self assembly, the Pt^{4+} can be uniformly distributed along the ACNT arrays. Pt^{4+} cations were then reduced to Pt metal in H_2 atmosphere. It was found that Pt-NPs growth due to the Ostwald sintering has been successfully prevented and geometry of ACNTs has been well-maintained (also see Fig. 2a).

3.2. Electron microscopic analyses of Pt-ACNTs

Scanning and transmission electron microscopic (SEM and TEM) analyses were conducted to understand the morphology and dispersion of Pt-decorated ACNTs due to the important role to secure the high performance and long-term stability of the electrocatalyst. The SEM cross-sectional image of Pt-ACNTs (Fig. 2a) indicated that dense and uniform ACNTs were highly aligned when the seed of iron (Fe) catalyst was used. After Pt-decoration through the feasible amphiphilic wet-chemistry approach, the ACNT highly aligned geometry is well-maintained. This alignment is highly beneficial to channeling the gas flow more efficiently. SEM micrographs of the Pt-ACNT catalyst also show Pt-NPs uniformly embedded along the ACNT surface, with a diameter ranging from 2 to 4 nm without further aggregation (Fig. 2b). The highly dispersed Pt-NPs suggested a large fraction of Pt atoms located at the surface of the ACNTs supports. High dispersion of Pt-NPs draws our attention for two reasons. First of all, high dispersion mitigates the usage of expensive metal (Pt). Secondly, the tunable particle sizes provide controllable structure, which in turn improves the PEMFC performance. The Pt-ACNT cathode catalysts are composed of multi-walled nanotubes with 5–19 layers. The SEM results also indicate that the oriented and uniform ACNTs arrays act as a support for cathodic catalyst to facilitate the O_2 gas diffusion. The improved specific surface areas of Pt-ACNTs advanced O_2 chemisorption and then increased the PEMFCs intrinsic reaction rates.

The high-resolution TEM images of Pt-ACNTs cathode catalyst were also obtained (Fig. 3a–d) to evaluate the geometry and alignment of Pt-ACNT, and the Pt nanoparticles and their size distribution. Selected TEM images (Fig. 3a and b) show the ACNTs have an average length of about 10 μm and a diameter of outer layer varying from 3.5 to 12.5 nm. The results indicated that the thickness of ACNT layer thickness was comparable to that of a conventional membrane electrode assembly (MEA). From our experimental data, it can be concluded that morphology of PEMFCs catalyst can efficiently channel the gas (H_2 and O_2) distribution, and in turn improve the electrochemical kinetics of PEMFC devices. The CVD-derived ACNTs consist of multiple concentric tubes with the interlayer distance approximately 0.396 nm (Fig. 3c), slightly larger than the interlayer distance in graphite. This observation evidently suggested that decoration of the ACNT occurred on the surface without insertion of the Pt-NPs (averaged size 2.7 nm) into the inner ACNT layers due to the size effect. These SEM/TEM images corroborate that the ACNTs provide ordered inter-tube spacing, thereby, greatly facilitating gas diffusion. Under carefully controlled fabrication conditions, the length and diameter of the Pt-ACNT can be adjusted to yield optimal catalytic surface area [55,56]. This observation corroborates that the high electrochemical activity of the PEMFCs devices can be achieved (see Fig. 6 and related discussion). From the ring pattern indexing, it can be seen that crystalline phase of Pt-NPs and ACNTs were obtained. The Pt ring patterns (Fig. 3d) were very well aligned with the

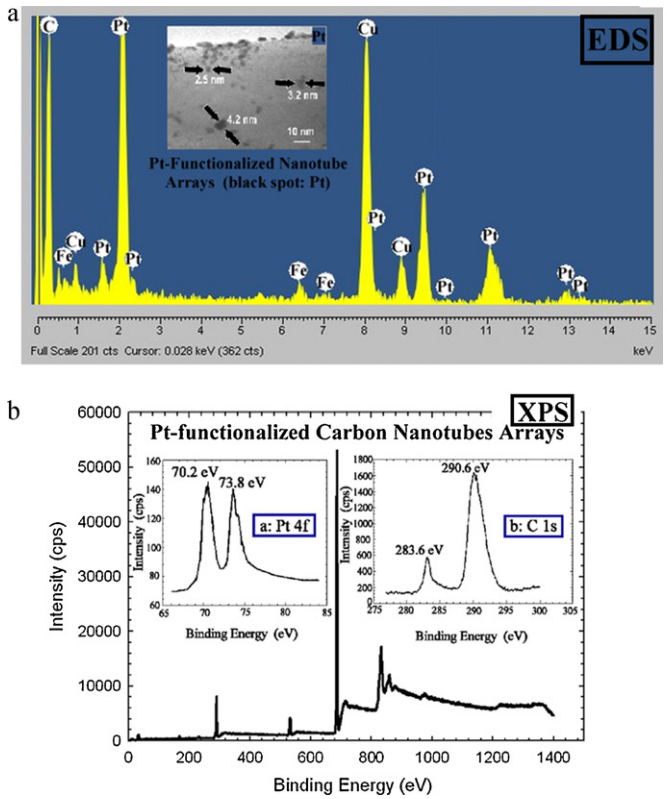

Fig. 4. Elemental composition analyses of the MEA composed of Pt-functionalized ACNT. (a) EDS analyses and (b) XPS analyses.

standard face-centered cubic of Pt (PDF 00-004-0802, 3.924 Å and 90°).

3.3. Elemental composition analyses of Pt-ACNTs

X-ray energy dispersive spectroscopy (EDS) and X-ray photoelectron spectroscopy (XPS) have been used as complementary techniques to confirm the stoichiometric Pt loading, ranging from 0.14 to 0.17 mg cm^{-2}, accordingly (Fig. 4a and b). EDS results indicated the principle emission of Pt occurs at M_α at 2.048 keV and L_α at 9.441 keV, correspondingly. The XPS full spectra indicated the presence of the Pt and C elements, well indexed by their standard spectra for 4f and 1s electron configurations, respectively. The emissions at 283.6 eV and 290.6 eV were attributed to the C=C double bonds in the ACNT arrays. Metallic Pt can be characterized by asymmetric emission lines with peak tailing to the binding energy (BE) corresponding to its innermost 4f electron excitation (BEs of $4f_{7/2}$ located at 72.1 eV and $4f_{5/2}$ at 76.4 eV) with peak splitting 4.3 eV. The composition analyses indicate that Pt loading can be decreased to 0.2 mg cm^{-2} while the high power density of the PEMFCs was maintained nicely. From the characteristic binding energy for C and Pt, it can be concluded that functionalization of ACNT by Pt is carried out through van der Waals intermolecular forces, without breaking C=C double bonds. The mono-dispersion of ultrafine Pt-NPs proves that decreased amount of Pt usage (<0.2 mg cm^{-2}) provides many electrochemically active sites, which consequently advance the PEMFC electrochemical performance.

3.4. Raman spectroscopic analyses of Pt-ACNTs

The characteristic spectra, radial breathing mode (RMB), D-band and G-band of a series of Pt-ACNT catalysts were evaluated by Raman spectroscopy. The results for six selected MEAs made

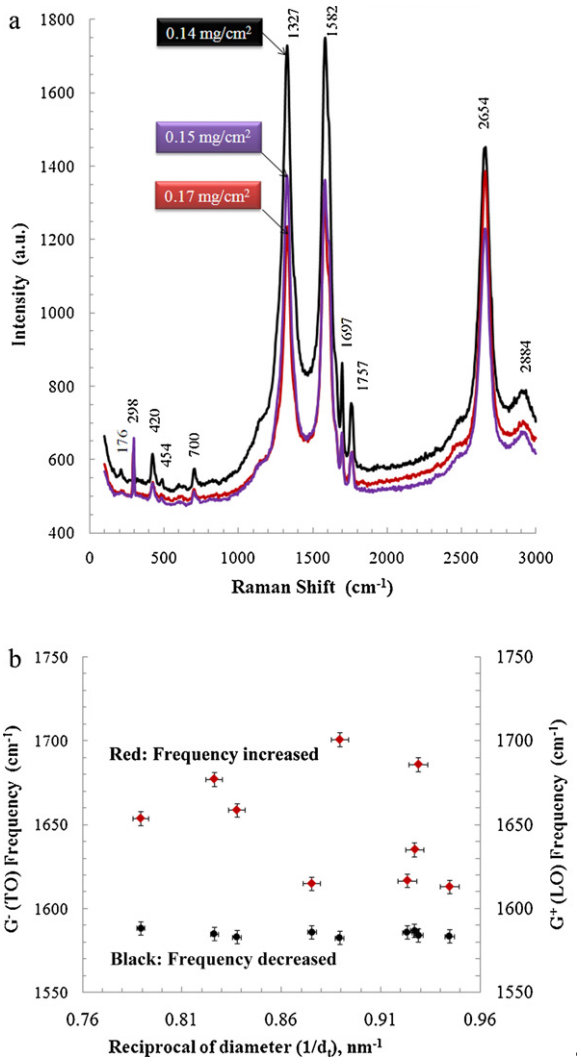

Fig. 5. Raman spectroscopic analyses of the Pt-functionalized ACNT at 633 nm excitation. (a) The spectroscopy to demonstrating the molecular vibration and (b) the G-band splitting due to the curvature effect.

from the Pt-ACNTs are consistent with standards of Pt and carbon nanotubes (Fig. 5a and b). The Pt metal displays two characteristic spectra at frequency of 483.24 cm^{-1} and 2084.98 cm^{-1}. The intensity of Pt is significantly low, confirming its small amount of loading. The main Raman features for carbon nanotubes are D band at 1250–1350 cm^{-1} and G band at about 1600 cm^{-1} (Fig. 5a). The Pt-decorated ACNTs displayed high intensity D band, suggesting that the strengthening of the D band is enhanced by Pt-NPs. This observation reveals the incorporation of platinum into carbon nanotubes. Meanwhile, the blue shift of D band to about 1315.10–1325.77 cm^{-1} occurred, suggesting the presence of crystalline graphite-like CNT was formed since it has a typical position of 1305–1330 cm^{-1} [40]. This measurement is in agreement to the reported data [57,58] that these second order Raman features are resulting from defect-induced and double resonance of Pt-ACNTs. The Pt-decorated ACNTs exhibited tangential vibrational modes, which results from the in-plane optic phonon mode. This phenomenon corresponds to the stretching mode of sp^2 hybridization in carbon nanotubes [59,60]. The G band was split into a lower frequency (G^-, 1584.17 cm^{-1}) and higher frequency (G^+, 1609.28 cm^{-1}), and this splitting is corresponding to the reciprocal of the interlayer of nanotubes as shown in Fig. 5b. The softening of G^- (TO) band, whose vibration perpendicular to the ACNT tubes,

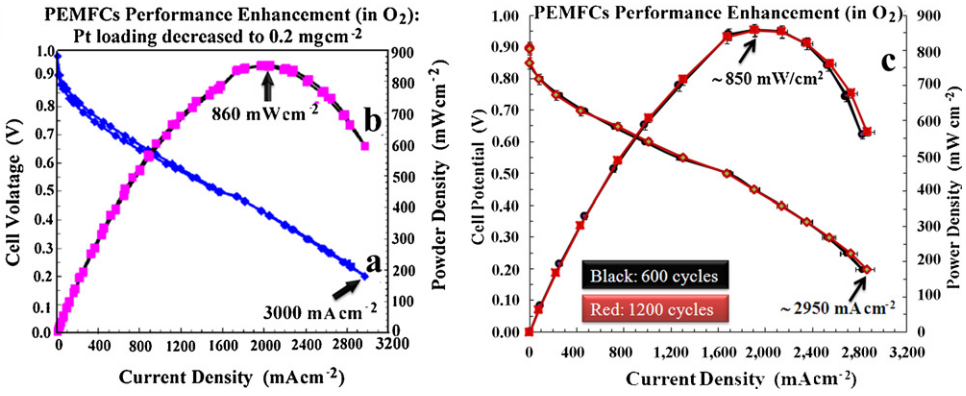

Fig. 6. Electrochemical performance of PEMFC device using Pt-ACNT as cathode catalyst. (a) Current density in O_2; (b) power density in O_2; (c) stability of PEMFC devices.

occurs due to the curvature in the Pt-ACNT. On the other hand, the strengthening of the G^+ (TO) band was observed due to its vibration along the ACNT tubes. The intermediate frequency mode (IFM) also occurred at 702.73 cm^{-1} due to the defect in the Pt-ACNTs. Importantly, it can be seen the "radial breathing mode" (RBM) of Pt-ACNT occurred at a lower frequency, ranging from 102.4 to 298.98 cm^{-1}. From the RBM determination, more accurate diameter calculation on CNTs can be obtained [61]. It was found that the diameter of CNT is inversely proportional to the Raman shift as demonstrated in Eq. (1):

$$\omega_{RBM} = \frac{A}{d_t} + B \quad (1)$$

where ω_{RBM} represents the radial breathing mode in cm^{-1}, d_t is the diameter of the ACNT in nm, A is a dimensionless constant (commonly used value is 218.2) and B is also an empirical constant (19.6 cm^{-1}), corresponding to the Raman shift.

Generally, an increase in the CNT diameter would result in a decrease in the RBM frequency [55–58]. It has to be noted that some satellite spectra were also seen due to the complexity of the MEA elemental composition and structure. Most importantly, the mode frequency of ACNTs and Pt depends on the laser excitation and the dimensional confinement.

3.5. Electrochemical performance of PEMFCs devices

The electrochemical performances of both Pt-ACNT and commercial ink-based PEMFCs were evaluated using cell current–potential polarization curves under identical operating condition. The DC polarization was conducted to identify the current density when potentials (0.2–1.0 V) were applied.

The current generally varies for different MEA specimens with the low Pt loading (about 0.2 mg cm^{-2}). The average current density at 0.2 V from six selected Pt-ACNT MEA specimens was 3200 mA cm^{-2} when O_2 is introduced into the cathode chamber (Fig. 6a). The PEMFC power density can be calculated by multiplying the cell potential with associated cell current density. The Pt-ACNT MEA displays a respectable peak power density of 625 mW cm^{-2} in air [62] and 860 mW cm^{-2} in oxygen (Fig. 6b). The various Pt-ACNT MEAs were tested and we found that the reproducibility of polarization over Pt-ACNT MEAs can be improved via tuning the geometry and structure of the nanotubes and Pt catalyst, although the variation is not as high as in some studies (reviewed by Gasteiger et al.) [21]. The stability of the same Pt-ACNT MEAs was determined at potential ranging from 0.2 to 1.0 V with a sweep rate at 5 s/cycle (Fig. 6c) over about 7200 cycles. Over the measured cycles, the relative deviations in the polarization curves were negligible, suggesting high PEMFC MEA stability. In this study, the polarization curves within 600–1200 cycles were arbitrarily selected to demonstrate stability. The current density at 0.2 V was maintained at 2860–2950 mA cm^{-2} ($\sigma < \pm 1.5\%$) and peak powder density was maintained within 850–860 mW cm^{-2} ($\sigma < \pm 0.6\%$), suggesting high stability of the PEMFC devices when operating in the O_2 atmosphere [27]. High stability and power/current densities are necessary when the fuel cell is required to withstand high dynamic load. It is important to point out that the Pt usage in this study was decreased to lower than 0.2 mg cm^{-2} determined by XPS analyses. The mass activity $i_{m(0.9V)}$ and specific activity $i_{s(0.9V)}$ at 0.9 V, though not measured here, have been previously reported by Liu et al. over Pt-ACNT cathode with the values being 101 A g_{Pt}^{-1} and 374 μA cm_{Pt}^{-2}, respectively [62].

During this study, we also found a key drawback of ACNT prepared by flowing catalyst method, which produce high level of iron (Fe) over the CNTs. Fe could be oxidized and affected Nafion membrane conductivity during fuel cell operation. Such shortcoming, however, can be mitigated by using ACNT prepared by a different method.

For comparison purposes, a side-by-side single-cell polarization study was carried out over Pt-ACNT PEMFCs and conventional ink-based PEMFCs. The operating conditions were the same as previously described with operating temperature at 75 °C, using humidified H_2 as fuel supply, and O_2 and air as oxidant. When air is used as the oxidant, the peak power density for commercial ink-based PEMFC reaches 281 mW cm^{-2} at $V = 0.35$ V (Fig. 7a). The Pt-ACNT PEMFCs, however, displayed a peak power density of 625 mW cm^{-2} under the same condition. In oxygen atmosphere, the peak power density for commercial ink-based PEMFC reaches 470 mW cm^{-2} at $V = 0.4$ V (Fig. 7b), where the Pt-ACNT PEMFCs displayed a peak power density of 860 mW cm^{-2} under the same condition.

From the performance comparison, it can be concluded that the Pt-ACNT PEMFCs exhibited similar performance to that of conventional ink-based PEMFCs in the low current region, where PEMFCs are generally designed to operate for the optimal energy conversion efficiency. However, the current and power densities have exceeded that of the conventional ink-based MEA at low voltage, and high output region. This observation further confirms our design goal that the alignment of the ACNT would lead to an enhancement in current and power densities through improved mass transfer. We pointed out, however, that our ink-based MEA was limited only by the one from the commercial source. Others have reported better performances under various conditions, as can be found in Refs. [21,63].

From the results comparison, it can safely be concluded that the alignment of carbon nanotubes contributed to performance improvement of the PEMFCs. Such gains are primarily from improved mass-transfer of gas flow and better conductance between the MEA and current collector by Pt-ACNTs being in

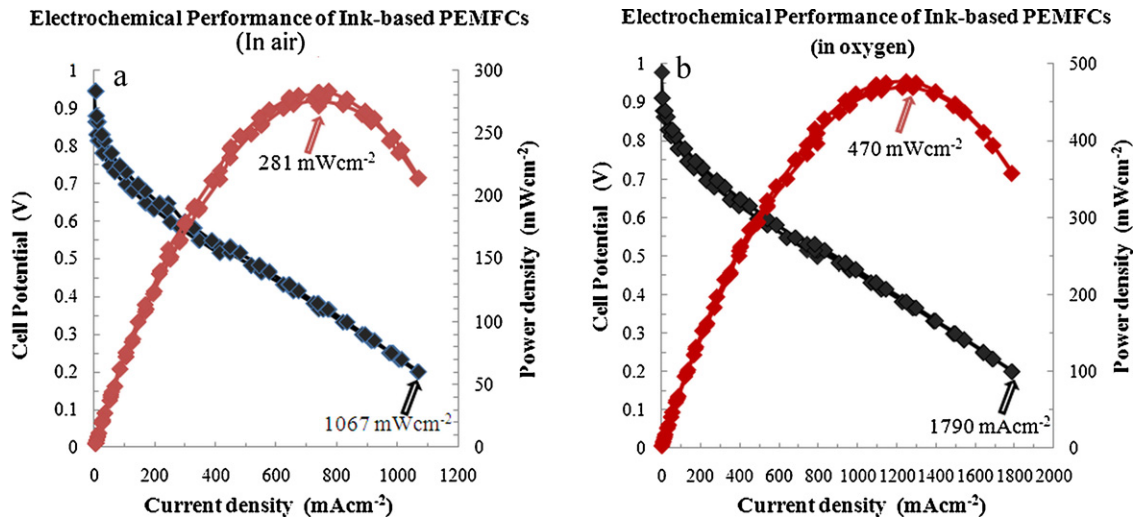

Fig. 7. Electrochemical performance of PEMFC device using conventional ink-based as cathode catalyst. (a) current density and power density in air and (b) current density and power density O_2.

aligned geometry. In addition, the alignment of ACNT also allows for channeling gas diffusion more efficiently compared with the traditional Pt-C catalysts. These inherent design features allow for substantial increase in reaction rates at the catalytic surface of the Pt-ACNT PEMFCs towards meeting the high power/current density requirements, in addition to the twin benefits of high utilization of the available Pt based catalyst due to the large specific surface area, aiding fast kinetics. Collectively, these benefits allow for the PEMFCs electrochemical behaviour to be advanced and the practical realization of PEMFC based devices in automobiles to be furthered along the roadmap.

4. Conclusions

The Pt-ACNT cathodic catalyst was obtained by chemical vapor deposition, followed by wet chemistry impregnation to decorate the catalyst, and heat treatment to activate the catalyst. The catalyst was characterized through SEM, TEM, and Raman spectroscopy. The results show that uniform ACNTs coated with Pt mono-dispersive NPs have been directly grown on cathode materials. The observed diameter of the ACNTs ranges from 5 to 20 nm and their lengths averaged 10 μm, depending on the growth time period. The Pt NPs are well dispersed on the surface of ACNTs and their size ranges from 2 to 4 nm. Additionally, the PEMFC performance tests indicate the maximum power density of PEMFC at 860 mW cm^{-2} and current density at 3200 mA cm^{-2} with the Pt NPs loading less than 0.2 mg cm^{-2} when the O_2 was used as the oxidant.

Acknowledgements

The authors are grateful to the National Science Foundation (NSF) Centers of Research Excellence in Science and Technology (NSF CREST, HRD-0734850) at the Texas A&M University-Kingsville, U. S. Department of Energy (DOE), the Office of Science, the Divisions of Educational Programs, Chemical Sciences and Engineering at the Argonne National Laboratory (ANL), and China Scholarship Council. The Faculty and Student Team (FaST) program collectively funded by NSF and DOE is duly acknowledged. The ACNT-MEA research at ANL was supported by DOE Office of Energy Efficiency and Renewable Energy, Fuel Cell Technologies Program. The assistance and support from Argonne National Fuel Cell group members, the discussion with Dr. Yang from the ANL, Dr. Liang and Dr. Young's from Texas A&M University (TAMU)-College Station and access to the facility at Materials Characterization Center at TAMU are also duly acknowledged. Finally, Dr. Hayes was acknowledged for copy-editing this manuscript.

Author contributions: Y. Yuan undertook SEM and RAMAN data analyses. She also co-wrote the manuscript. J. Smith participated in this project as a FaST student fellow. He was trained to prepare carbon nanotubes and modify the ACNTs using platinum precursors. G. Goenaga conducted the student training and optimized the ACNTs fabrication variables. D.-J. Liu was the principal investigator of a DOE funded project of using ACNT as fuel cell electrode support. He is responsible for the concept development, design of experiment and project execution. He hosted the FaST fellows during their research at Argonne National Laboratory. Z. Luo collected the TEM images and EDS elemental compositions. J. Liu was temporarily employed at the Argonne National Laboratory as a FaST faculty fellow. All authors edited and proof-read this manuscript. D.-J. Liu and J. Liu also oversaw the project progress. Finally, J. Liu is responsible for submitting the manuscript and related figures.

References

[1] S. Moghaddam, E. Pengwang, Y. Jiang, R. Garcia, D.J. Burnett, C.J. Brinker, R.I. Masel, M.A. Shannon, Nat. Nanotechnol. 5 (2010) 230–236.
[2] R. Esposito, A. Conti, Polymer Electrolyte Membrane Fuel Cells and Electrocatalysts, Nova Science Publisher, New York, 2009.
[3] H.W. Cooper, Chem. Eng. Prog. 103 (2007) 34–43.
[4] S.K. Buratto, Nat. Nanotechnol. 5 (2010) 176.
[5] G.J. O' La, H.J. In, E. Crumlin, G. Barbastathis, Y. Shao-Horn, Int. J. Energy Res. 31 (2007) 548–575.
[6] J.D. Morse, Int. J. Energy Res. 31 (2007) 576–602.
[7] J. Jagur-Grodzinski, Polym. Adv. Technol. 18 (2007) 785–799.
[8] J. Pan, S. Lu, Y. Li, A. Huang, L. Zhuang, J. Lu, Adv. Funct. Mater. 20 (2010) 312–319.
[9] J. Larminie, A. Dicks, Fuel Cell Systems Explained, second ed., John Wiley & Sons Ltd., London, 2003.
[10] S. Gamburzev, A.J. Appleby, J. Power Sources 107 (2002) 5–7.
[11] J.J. Baschuk, X. Li, Int. J. Energy Res. 27 (2003) 1095–1116.
[12] A. Kazim, P. Forges, H.T. Liu, Int. J. Energy Res. 27 (2003) 401–414.
[13] M.A. Hickner, B.S. Pivovar, Fuel Cells 5 (2005) 213–229.
[14] H. Yu, B. Yi, Fuel Cells 4 (2004) 96–100.
[15] C. Wang, M. Waje, X. Wang, J.M. Tang, R.C. Haddon, Y. Yan, Nano Lett. 4 (2004) 345–348.
[16] G. Hörmandinger, N.D. Lucas, Int. J. Energy Res. 21 (1997) 495–526.
[17] P.M. Gomadam, J.W. Weidner, Int. J. Energy Res. 29 (2005) 1133–1151.
[18] J.F. Lin, V. Kamavaram, A.M. Kannan, J. Power Sources 195 (2010) 466–470.
[19] V. Kamavaram, V. Veedu, A.M. Kannan, J. Power Sources 188 (2009) 51–56.
[20] M.B. Fischback, J.K. Youn, X. Zhao, P. Wang, H.G. Park, H.N. Chang, J. Kim, S. Ha, Electroanalysis 18 (2006) 2016–2022.
[21] H.A. Gasteiger, S.S. Kocha, B. Sompalli, F.T. Wagner, Appl. Catal. B 56 (2005) 9–35.
[22] V. Mazumder, Y. Lee, S. Sun, Adv. Funct. Mater. 20 (2010) 1224–1231.

[23] V. Di Noto, E. Negro, R. Gliubitszzi, S. Lavina, G. Pace, S. Gross, C. Maccato, Adv. Funct. Mater. 17 (2007) 3626–3638.
[24] X. Huang, R. Solasi, Y. Zou, M. Feshler, K. Reifsnider, D. Condit, S. Burlatsky, T. Madden, J. Polym. Sci. Part B: Polym. Phys. 44 (2006) 2346–2357.
[25] Y. Shao, G. Yin, Z. Wang, Y. Gao, J. Power Sources 167 (2007) 235–242.
[26] H. Chu, Y. Shen, L. Lin, X. Qin, G. Feng, Z. Lin, J. Wang, H. Liu, Y. Li, Adv. Funct. Mater. 20 (2010) 3747–3752.
[27] J. Yang, G. Goenaga, A. Call, D.-J. Liu, Electrochem. Solid State Lett. 13B (2010) 55–57.
[28] A.L. Dicks, The role of carbon in fuel cells, J. Power Sources 156 (2006) 128–141.
[29] A.M. Yashchenok, D.N. Bratashov, D.A. Gorin, M.V. Lomova, A.M. Pavlov, A.V. Sapelkin, B. Sup Shim, G.B. Khomutov, N.A. Kotov, G.B. Sukhorukov, H. Möhwald, A.G. Skirtach, Adv. Funct. Mater. 20 (2010) 3136–3142.
[30] X. Yu, S. Ye, J. Power Sources 172 (2007) 133–154.
[31] J. Sung, J. Huh, J. Choi, S.J. Kang, Y.S. Choi, G.T. Lee, J. Cho, J. Myoung, C. Park, Adv. Funct. Mater. 20 (2010) 4305–4313.
[32] T.W. Ebbesen, P.M. Ajayan, Nature 358 (1992) 220–222.
[33] Y. Chen, Z. Iqbal, S. Mitra, Adv. Funct. Mater. 17 (2007) 3946–3951.
[34] C.C. Chen, C.F. Chen, C.H. Hsu, I.H. Li, Diamond Relat. Mater. 14 (2005) 770–773.
[35] M. Paradise, T. Goswami, Mater. Des. 28 (2007) 1477–1489.
[36] F.N. Büchi, S. Srinivasan, J. Electrochem. Soc. 144 (1997) 2767–2772.
[37] J. Yang, D.-J. Liu, Carbon 45 (2007) 2843–2854.
[38] J.J. Baschuk, X. Li, J. Power Sources 86 (2000) 181–196.
[39] S.M. Alia, G. Zhang, D. Kisailus, D. Li, S. Gu, K. Jensen, Y. Yan, Adv. Funct. Mater. 20 (2010) 3742–3746.
[40] R. Yu, L. Chen, Q. Liu, J. Lin, K. Tan, S. Ng, O.H.S. Chan, G.Q. Xu, T.S.A. Hor, Chem. Mater. 10 (1998) 718–722.
[41] P.R. Poulsen, J. Borggreen, J. Nygard, D.H. Cobden, M.M. Andreasen, P.E. Lindelof, American Institute of Physics (AIP) Conference Proceedings, Kirchberg, Tirol (Austria), 4–11 March, 2000 (Available from: http://faculty.washington.edu/cobden/DHCpapers/Poulsen00.pdf).
[42] Z. He, J. Chen, D. Liu, H. Zhou, Y. Kuang, Diamond Relat. Mater. 13 (2004) 1764–1770.
[43] K. Kinoshita, J. Electrochem. Soc. 137 (1990) 845–848.
[44] Y.Y. Shao, G.P. Yin, Y.Z. Gao, J. Power Sources 171 (2007) 558–566.
[45] J.G. Liu, Z.H. Zhou, X.X. Zhao, Q. Xin, G.Q. Sun, B.L. Yi, Phys. Chem. Chem. Phys. 6 (2004) 134–137.
[46] C.P. Deck, K. Vecchio, Carbon 43 (2005) 2608–2617.
[47] S.B. Sinnott, R. Andrews, D. Qian, A.M. Rao, Z. Mao, E.C. Dickey, Chem. Phys. Lett. 315 (1999) 25–30.
[48] R.T.K. Baker, P.S. Harris, in: P.L. Walker, P.A. Thrower (Eds.) Chem. Phys. Carbon 14 (1978) 83–165.
[49] S.D. Miguel, O. Scelza, M. Romanmartinez, C. Salinas-Martinez, D. Cazorla-Amoros, A. Linares-Solano, Appl. Catal. A: Gen. 170 (1998) 93–103.
[50] N. Giordano, E. Passalacqua, L. Pino, A.S. Arico, V. Antonucciv, M. Vialdi, K. Kinoshita, Electrochim. Acta 36 (1991) 1979–1984.
[51] T. Belin, F. Epron, Mater. Eng. B 119 (2005) 105–118.
[52] D.-J. Liu, J. Yang, D.J. Gosztola, ECS Trans. 5 (2007) 147–154.
[53] G.G. Wildgoose, C.E. Banks, R.G. Compton, Small 2 (2006) 182–193.
[54] Z.P. Luo, Acta. Mater. 54 (2006) 47–58.
[55] K. Lee, J.J. Zhang, H.J. Wang, D.P. Wilkinson, J. Appl. Electrochem. 36 (2006) 507–522.
[56] X. Teng, X. Liang, S.N. Maksimuk, H. Yang, Small 2 (2006) 249–253.
[57] M.S. Dresselhaus, G. Dresselhaus, R. Saito, A. Jorio, Phys. Rep. 409 (2005) 47–100.
[58] L.M. Malard, M.A. Pimenta, G. Dresselhaus, M.S. Dresselhaus, Phys. Rep. 473 (2009) 51–87.
[59] M.S. Dresselhaus, A. Jorio, M. Hofmann, G. Dresselhaus, R. Saito, Nano Lett. 10 (2010) 751–758.
[60] L.G. Cancado, A. Hartschuh, L. Novotny, J. Raman Spectrosc. 40 (2009) 1420–1426.
[61] A.A. Green, M. Hersam, Nat. Nanotechnol. 4 (2009) 64–70.
[62] D.-J. Liu, J. Yang, N. Kariuki, G. Goenaga, A. Call, D. Myers, ECS Trans. 16 (2) (2008) 1123–1129.
[63] H.A. Gasteiger, J.E. Panels, S.G. Yan, J. Power Sources 127 (2004) 162–171.